Chapter 4

Case study at the German Continental Deep Drilling Site (KTB): Mutual relationship between microseismicity and seismic reflectivity

Two fluid injection experiments were conducted at the German Continental Deep Drilling site (KTB) in 1994 and 2000. Microseismicity occurred at different depth intervals. Hypocenter locations were precisely localized. Here, microseismicity is analyzed in terms of its spatio-temporal evolution. The SBRC approach is applied which assumes that microseismicity is triggered by a diffusive process of pore pressure relaxation. The method yields estimates of hydraulic parameters of rocks on large spatial scales. At the KTB site the method enables us to study hydraulic diffusivity at two different depth intervals under the unique conditions of a superdeep borehole. Significant variations in the evolution characteristics of the seismic activity at different depths are observed. Estimates of hydraulic diffusivity for shallower parts of the crust are much smaller than for deeper regions. To understand the reasons for this, the spatial relation of hypocenter locations to the distribution of seismic reflection intensities are analyzed. Low values of hydraulic diffusivity correlate with low reflection intensities and vice versa. The analysis confirms the hypothesis that the process of pore pressure relaxation along pre-existing and critically stressed natural fractures is an important triggering factor for induced microseismicity.

4.1 Introduction

The German Continental Deep Drilling site (KTB) is located in SE Germany near the western margin of the Bohemian Massif at the contact zone of the Saxothuringian and the Moldanubian (Wagner et al. [1997]). The geological set-up as well as the drilling location is shown in figure 4.1. Two boreholes were drilled within a crustal segment mainly composed of metabasites and gneisses (Pechnig et al. [1997]). The pilot hole reached a maximum depth of 4 km whereas the main hole penetrated down to 9.1 km. Drilling was finished in 1994. During the following years, extensive research was conducted at the KTB. In order to study fluid transport processes at the KTB and to obtain knowledge about crustal stresses, a short-term fluid injection experiment was carried out in 1994 (Zoback and Harjes [1997a]; Jost et al. [1998]). In 2000 a long-term fluid-injection experiment was performed at the KTB. For details of this experiment refer to Baisch et al. [2002], Baisch and Harjes [2003] and Bohnhoff et al. [2003].

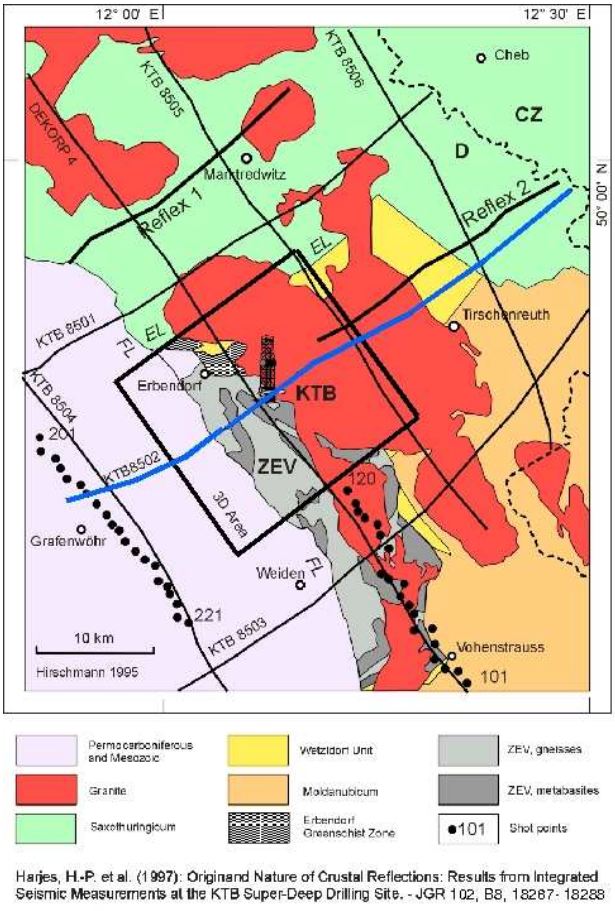

Figure 4.1: Location of the German Continental Deep Drilling site in SE Germany at the contact zone of the Saxothuringian and the Moldanubian (from Harjes et al. [1997]). Besides the drilling location and the geological units, the location of seismic profiles are shown. The blue line corresponds to the 2D seismic reflection profile `KTB8502`, the black rectangular area denotes the 3D reflection profile `ISO89-3D`.

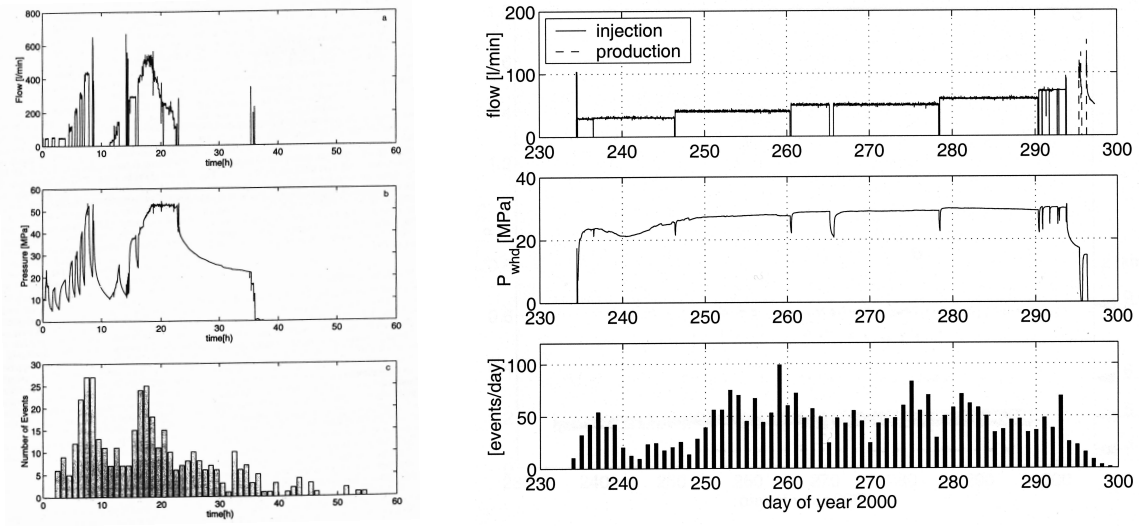

(a) (b)

Figure 4.2: Injection rate (top), well head pressure (middle) and rate of induced events (bottom) as a function of time for the KTB fluid-injection experiment in (a) 1994 and (b) 2000. Taken from Zoback and Harjes [1997b] and Baisch and Harjes [2003].

During the fluid-injection experiment in 1994 about 200 m^3 of KBr/KCl brine were injected at the open hole section within 24 hours (see figure 4.2a, top). 73 surface seismometers and one 3-component borehole seismometer recorded approximately 400 microearthquakes within 60 hours after the fluid injection (figure 4.2a, bottom). All events were considered to be induced by the injected fluids (Zoback and Harjes [1997a]). 94 of these earthquakes could be localized with respect to master events with a relative location accuracy of several 10's of meters (Bohnhoff et al. [2003]). Later, the data was precisely relocalized using various hypocenter location improvements (Baisch et al. [2002]). The seismically active zone comprises a volume of approximately 0.35 km^3 around the bottom of the borehole. Only a small increase in pore pressure (< 1 MPa) was sufficient to trigger the earthquakes. Surprisingly, only events above 9100 m were observed. Possible explanations were given by Zoback and Harjes [1997a]: either the occurrence of the brittle-ductile transition zone at this depth (impermeable half-space) and/or a decreased stress level much smaller than the rock's frictional strength.

The injection experiment of 2000 was designed to enable fluid migration farther away from the injection interval and to cause pore pressure increase also at larger distances. During this long-term injection experiment, about 4000 m^3 of water were injected at the wellhead of the main borehole at injection rates of 30-70 l/min (Baisch et al. [2002]; see figure 4.2b, top). A temporary seismic network consisting of a borehole seismometer in the pilot hole at 3827m depth and a surface network of 39 stations was installed (Bohnhoff et al. [2003]). About 2800 microseismic events were detected of which 237 where localized with an accuracy better than 100m on average (figure 4.2b, bottom). Since preceding hydraulic tests did not indicate any leaks in the casing, it was assumed that the main borehole was

hydraulically closed at least down to 6 km depth. However, due to several leakages in the borehole casing which were not known before, about 80% of the fluid was, in fact, injected between 5.35 and 5.4 km depth. Seismic events clustered at two depth levels of 5.0-6.0 km (81% of total seismicity) and 8.8-9.2 km (11% of total seismicity, Bohnhoff et al. [2003]; see figure 4.3(a) and 4.3(b)).

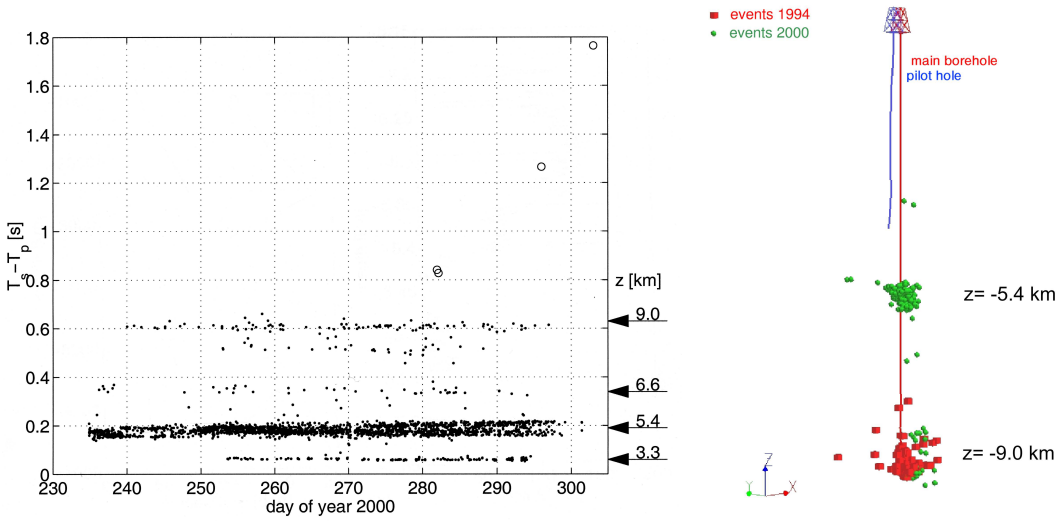

(a) (b)

Figure 4.3: (a) Difference of onset times of seismic P and S phase ($S-P$) plotted against time for injection-induced events recorded at a downhole seismometer during the experiment in 2000. Hypocentral depth estimates can be obtained directly by $S-P$ times (from Baisch and Harjes [2003]). (b) Location of seismic events induced during the two fluid injection experiment in 1994 and 2000 at the KTB site. Events triggered in 1994 are shown as red rectangles, events triggered in 2000 in green spheres.

To explain the triggering mechanism of microearthquakes during fluid injection experiments in general, it was proposed already by Healy et al. [1968] that increasing fluid pressure along pre-existing fractures can cause a reduction of the effective normal stress and initiate the release of tectonic stress. This explanation was further confirmed by Raleigh et al. [1976]. If pore pressure perturbations play a dominant role in the triggering mechanism, such a process is directly influenced by the hydraulic properties of the rocks. Therefore, the idea for developing an approach to estimate such properties on large spatial scales using induced microseismicity arises. Such a method was proposed with the SBRC and was already introduced in chapter 2. Here, it will be focused on the analysis of the data observed at the KTB.

In this study I concentrate on the analysis of the fluid-induced microseismicity at two different depth levels: During the 1994 injection experiment, about 100 microseismic events occurred around the open hole section at 8.0-9.1 km depth. During the 2000 experiment about 50 events were triggered at this depth level. Moreover, a major cloud of approximately 200 events was localized around 5.4 km depth (see figure 4.3(b)). The number of hypocenters for these two depth intervals are large enough to apply the SBRC method.

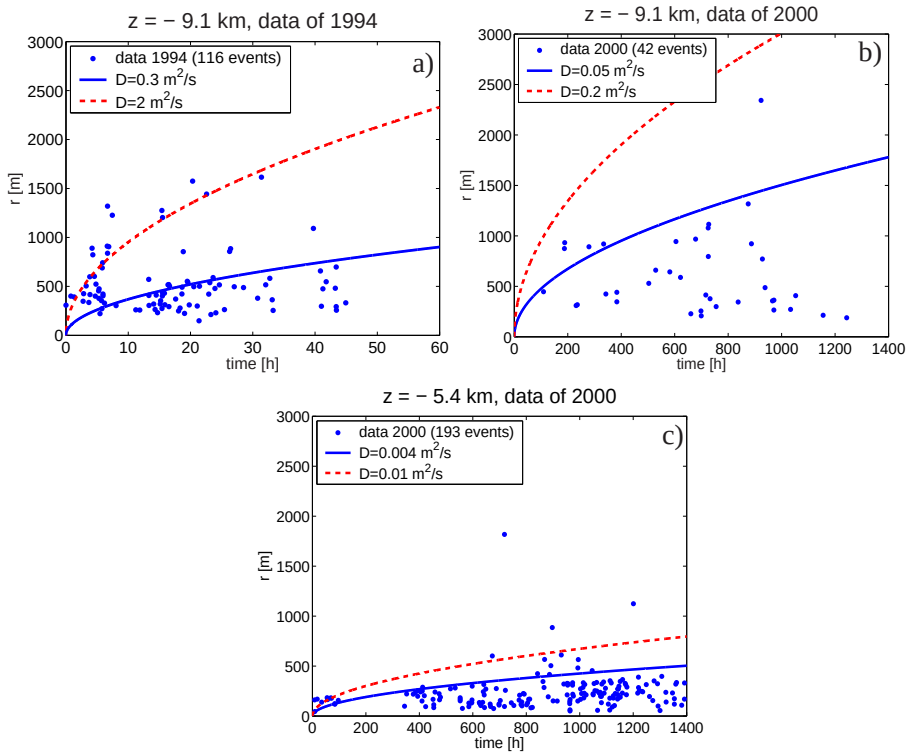

Figure 4.4: Estimation of the scalar hydraulic diffusivity for the two main depth domains where microseismicity occurred. a) Estimation for the depth domain around 9 km for data of 1994 and b) for 2000 data. c) Estimation for the depth domain around 5.4 km. In spite of the small event number, the magnitude of hydraulic diffusivity is found to be much lower in the shallower domain compared with the deeper domain. Note also the different time scale in figures a)and b).

4.2 Results of hydraulic diffusivity estimates

The 1994 data set has already been analyzed in terms of the SBRC method by Shapiro et al. [1997] using equation (2.6). Good agreement between equation (2.6) and the data was observed (see figure 4.4a). Estimates of hydraulic diffusivity for the depth interval at the open hole section vary between 0.3 m^2/s and 2 m^2/s. The order of magnitude estimates are in good agreement with independent estimates of hydraulic diffusivity of the crystalline crust (e.g. Scholz [1990]). A tensor of hydraulic diffusivity and permeability was estimated by Rindschwentner [2001]. The principal components of this tensor were found to be orientated quasi-parallel to the Franconian lineament, which continues through the upper crust as a highly reflective zone. This zone (seismic reflector SE1) was cut by the main borehole at approximately 6.8-7.2 km depth. Moreover, the horizontal projection of the main axes of the tensor were found to be parallel to the maximum horizontal principal stress with an orientation of N160°±10°E (Brudy et al. [1997]), which also corresponds well with a subhorizontal NS direction of the stress component σ_1 as determined from fault mechanisms of the microseismicity of the 2000 injection experiment (Bohnhoff et al. [2003]). For more details and further studies of the correlation of our results with stress tensors refer to chapter 4.5.

Equation (2.6) was applied to the data of the year 2000 experiment. For the analysis, the major fluid loss intervals obtained by flow logs (5.35km, 5.4km, 9.03km) were used as source locations.

As a first result, the estimates of hydraulic diffusivity for the lower depth interval of Shapiro et al. [1997] and Rindschwentner [2001] were confirmed (see figure 4.4b). For the year 2000 data values of hydraulic diffusivity of 0.05 m^2/s to 0.2 $m^2/s$are found, which are of the same order of magnitude as before. The slight differences are most likely due to the small event number. In contrast to the large values estimated for the larger depth at the KTB, the values of hydraulic diffusivity for the shallower depth interval at 5.4 km were found to be a factor 20 to 100 smaller than at 9.1 km (Figure 4.4c). In spite of the small event numbers this remarkable difference in diffusivity magnitude is significant. The largest diffusivity at the greatest depth is observed. This observation seems to be in disagreement with the fact that 80% of fluid was lost at the upper borehole interval. This can be explained by a local hydraulic heterogeneity close to the borehole. For example, there can be several small-scale open fractures or even a hydraulic contact to the fluid behind the casing. Such features can cause a large fluid loss without producing any seismicity (Baisch et al. [2002]; Baisch and Harjes [2003]). A local heterogeneity may lead to the effect that only a small part of these 80% was really injected into the seismically active rock volume. The hydraulic diffusivity estimations above have been obtained for the total seismic active zone. Here, it is assumed that these values are not affected by the properties of the small-scale features causing the large fluid loss.

Our results of hydraulic diffusivity estimates correlate very well with results obtained by Costain and Bollinger [1996]. For example, from quite a different approach Costain and Bollinger [1996] estimated a value of 1.6 m^2/s for the earths crustal diffusivity, in excellent agreement with our results at the KTB site. This agreement is remarkable because of the more indirect approach they used.

4.3 3D seismic reflection intensities

Before and during the drilling phase at the KTB site, intensive seismic studies were carried out. From a 2-D seismic survey (KTB8502), which was oriented perpendicular to the strike of the Franconian Lineament (FL), a sharp northeast-dipping seismic reflector zone (SE1) was identified in seismic profiles (Simon et al. [1996]; Harjes et al. [1997]; Buske [1999], see figure 4.5a). This reflector is regarded as the continuation of the FL through the upper crust. A prestack Kirchhoff depth migration of the KTB8502 profile as well as of a 3D seismic reflection survey (ISO89-3D) was presented by Buske [1999]. During the ISO89-3D experiment, an area of about 21 km $\times$ 21 km was investigated using reflection seismics. The main borehole is located at the center of this region. Figure 4.5 shows the relevant parts of profile ISO89-3D after a 3-D Kirchhoff migration (Buske [1999]). Beneath the SE1 reflector, in the depth range 11 to 14 km, a highly reflective region known as the Erbendorf Body (EB) can be observed. The 3D reflection intensities clearly show

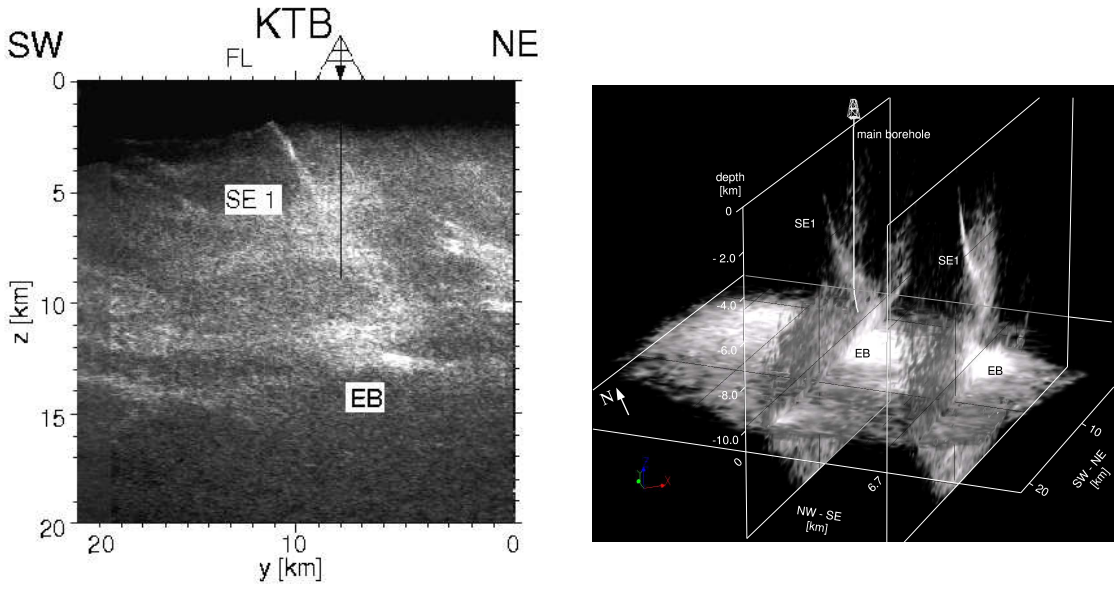

(a) (b)

Figure 4.5: (a) Part of the 2D pre-stack migration of the profile `KTB8502`, from Buske [1999]. (b) 3D pre-stack Kirchhoff depth migration of profile `ISO89-3D`. The seismic reflection intensities are shown in grayscale on three slices: one horizontal slice at 11 km depth and two vertical slices with an offset of 6.7 km. The left hand slice is passing through the location of the main borehole. Light colors correspond to large reflection intensities and darker colors with lower intensities. The SE1 reflector is clearly visible as a steeply dipping event. The EB appears with strong reflectivity at a depth of 10-14 km. The dimension of the whole migrated volume is $21 \times 21 \times 15$ km.

the geometry and the lateral extent of the SE1 reflector and the EB in the subsurface at a relatively high resolution.

4.4 Correlation of microseismicity and reflectivity

In order to clarify the results obtained by the SBRC method for data of the KTB injection experiments, hypocenter locations in relation to the 3D distribution of seismic reflection intensities are analyzed. Such a combined analysis may explain the significant differences in depth-dependent magnitudes of hydraulic diffusivity.

The hypocenter locations of microseismicity of 1994 and 2000 together with the migration results are shown in figure 4.6. The prominent seismic reflector SE1 is clearly visible as well as the Erbendorf Body at 11 km depth. From figure 4.6 it can be clearly observed that the upper microseismic cloud is spherical to a first order approximation. This can be explained by more or less isotropic hydraulic properties at this location. The entire cloud is concentrated within a relatively small region. Note that this part of the rock is char-

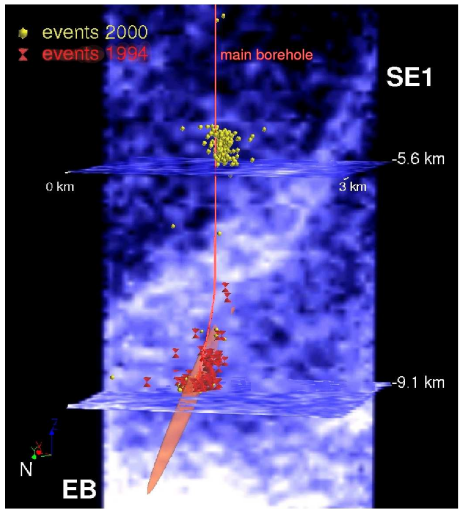

Figure 4.6: 3D migration (view from NW) together with the microseismic hypocenters (events 1994=red/dark tetrahedra, events 2000=yellow/light spheres, Baisch et al. [2002]) and the tensor of permeability estimated from the 1994 data set (Rindschwentner [2001]). The volume of rock where the sphere-shaped upper cloud occurred is characterized by comparatively low reflectivity. The lower cloud of events seems to be preferentially orientated along the directions of the highly reflective (SE1) zone.

acterized by a small hydraulic diffusivity. The seismic clouds which occurred around the open hole section of the main borehole in 1994 and 2000 are characterized by significantly more widespread hypocenter locations (yellow/light spheres and red/dark tetrahedra). The hypocenters are found to be strongly correlated with the dip of the SE1 reflector. The tensor of permeability is also shown in figure 4.6. It is characterized by strong anisotropy. Its principal axes are quasi-parallel to the SE1 fault zone.

The orientations of pre-existing fault structures and fractures affect the hydraulic diffusivity and the spatial distributions of the microseismicity clouds. The slices included in the migration image (Figure 4.6) show that the upper part of the rock is characterized by comparatively lower reflection intensities than the lower part. It can be clearly observed that the upper seismic cloud occurred within a depth domain that shows less reflectivity. The lower cloud occurred in a domain which is characterized by comparatively higher reflectivity. This observation is in agreement with the previous estimates of hydraulic diffusivity at the KTB: it is smaller in the upper part of the considered rock volume and larger in its lower part.

A model which may explain this correlation is the following: a rock volume characterized by an increased density of pre-existing fractures affects the propagation of seismic waves to a larger extent compared to a region containing less fractures. More seismic energy is reflected or backscattered from a highly fractured domain. In a pre-stack depth migration of seismic profiles these parts of the rock will be imaged as zones of increased seismic reflection intensity. Regions of the rock affecting the propagation of seismic waves to a lesser extent will be imaged as low-reflectivity zones. Therefore it is reasonable to conclude that shallower parts at the KTB site are characterized by less pre-existing natural fractures, correlating with smaller reflection intensities and smaller values of hydraulic dif-

fusivity. Deeper regions show comparatively higher reflection intensities and preferential aligned seismic hypocenters, correlating with large hydraulic diffusivities and more dense pre-existing, oriented fractures.

4.5 Correlation of seismic structures and microseismicity with stress tensor

The estimates of hydraulic diffusivity at the KTB yielded interesting results and helped to interpret the physical phenomenon of induced microseismicity. However, a comparison of our results with independent studies is necessary. As already mentioned in chapter 4.2, the horizontal projection of the main axes of the tensor of estimated hydraulic diffusivity or permeability were found to be parallel to the maximum horizontal principal stress with an orientation of N160°±10°E found by Brudy et al. [1997]. Moreover, Brudy et al. [1997] tried to verify the validity of both the applicability of laboratory derived strength parameters to the crust, and the assumption that the crust is in a state of failure equilibrium - relevant for the SBRC method. Therefore, they determined the complete stress tensor (the magnitude and orientation of the three principal stresses) using an 'integrated stress measurement strategy' to a depth of 8.6 km at the KTB. Their main results which are important for our

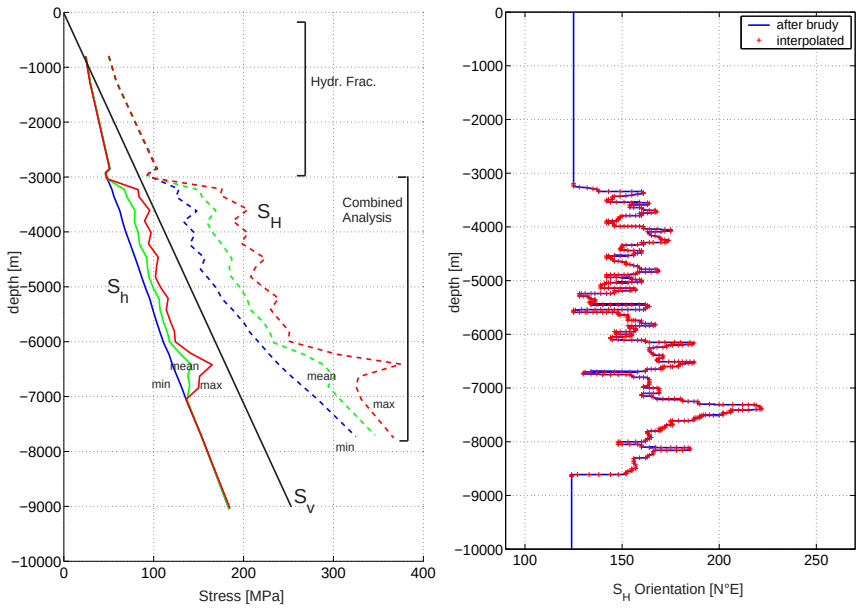

Figure 4.7: Stress tensor at the KTB with depth after Brudy et al. [1997]. Left: Stress magnitudes estimated using hydraulic fracturing and a combined analysis (compare figure 11 in Brudy et al. [1997] and the comments therin). S_H, S_h and S_v correspond to maximum and least principal horizontal and maximum vertical stress, respectively. Right: Profile of the orientation of maximum horizontal principal stress S_H in the depth section 3.2 km to 8.6 km using the most reliable stress orientation data from any depth. Except an abrupt change in stress orientation at about 7200m, the orientation of S_H is quite constant over the entire depth interval (figure 8 after Brudy et al. [1997])

purpose are shown in figure 4.7. Here, the estimated stress magnitudes using hydraulic fracture and the combined analysis is shown on the left. On the right, the profile of the orientation of maximum horizontal principal stress S_H in the depth section 3.2 km to 8.6 km using the most reliable stress orientation data is displayed (after figure 8 of the publication of Brudy et al. [1997]). The authors found that

> *[...] The observed orientation of the greatest horizontal principal stress S_H is remarkably uniform ($N150^oE$-$N170^oE$) along the entire investigated interval from 3.2km to 8.6km depth. Besides ubiquitous small-scale variations of the stress orientation, the only significant deviation from the overall trend is observed below 7.2km depth, where the lower bound of the intersection of the borehole with a major fault zone, the SE1 reflector, is located.*

The results found by Brudy et al. [1997] were also compared with our findings of the correlation of reflectivity and microseismicity. Therefore, the results were interpolated and transformed into a 3D-image of the depth-dependent stress tensors at the KTB. The results are shown in figure 4.8. Here, the depth-dependent stress tensor is shown together with microseismic events induced during the two injection experiments at the KTB and the seismic reflection amplitudes from three different views. Note, that the relative ratio of the tensor axes are according to figure 4.7 (left).

The remarkable deviation from the overall uniform trend is clearly visible at a depth of 7.2km (yellow tensor), where the orientation changes significantly and rapidly. Moreover, the arrangement of seismic hypocenters seems to be strongly correlated with the stress tensor magnitudes and orientations: In the shallower part (around 3 km and 5.4 km), the tensor components have nearly the same size, indicating a more spherical tensor correlating with a spherical distribution of hypocenters at these depths. In deeper regions (7.2 km and below), the tensor components are changing remarkably resulting in anisotropic stress tensors. Seismic hypocenters at these depth also show strong anisotropic distributions.

4.6 Modeling of microseismicity at the KTB

4.6.1 Injection signal and event number

Using the numerical model presented in chapter 3, fluid-induced microseismicity at the KTB was simulated. At first, the sensitivity of the microseismicity triggering on the pressure signal is studied. Therefore, the pressure perturbation measured during the 1994 injection experiment at the KTB is simulated with the modeling approach. A hydraulic homogeneous and isotropic 3D model is used. Criticality is evenly distributed as shown in chapter 3.4.1 (figure 3.6). The point source is located in the center of the medium. As boundary condition, the time-dependent pressure perturbation shown in figure 4.9a is used. The original profile of the signal is interpolated at the time steps used for modeling. The

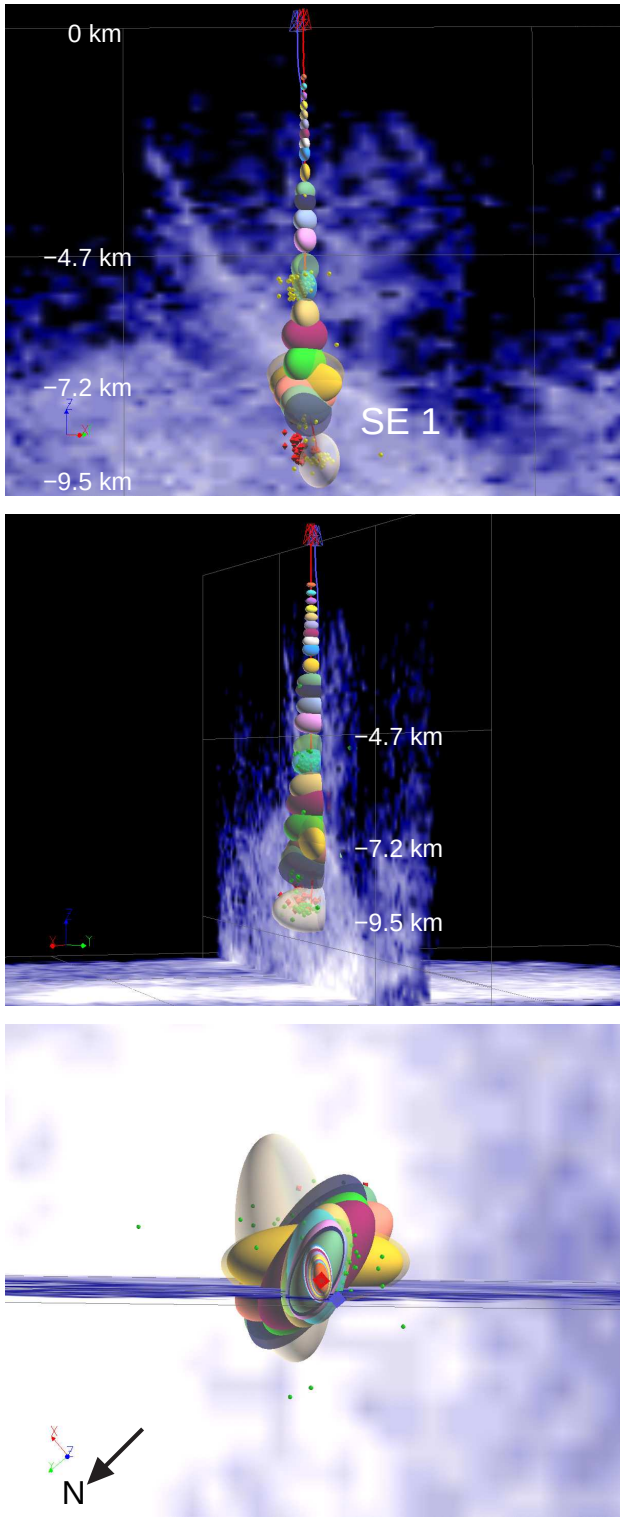

Figure 4.8: Depth-dependent stress tensor after Brudy et al. [1997] at the KTB site together with microseismic events induced during the two injection experiments and seismic reflection amplitudes. Top: view from south-west, middle: view from north-east, bottom: view from the top. Note the change in stress orientation at about 7200m. Elsewhere, the orientation of S_H is quite constant over the entire depth interval. Tensors are shown for every 200m for the depth interval 1 km to 2.6 km and at 3km, 3.4km, 3.6km, 4km, 4.4km, 5km, 5.4km, 6km, 6.4km, 7km, 7.2km, 7.4km, 7.6km, 7.8km, 8km and 9km.

comparison of figure 4.2a (top) and 4.9a clearly shows the adequate simulation of the real injection function.

The first aim of this study was the analysis of the change of event numbers triggered with time, i.e., event rate. The event rate observed during the 1994 experiment is shown in figure 4.2 (bottom). The measured event rate seems to be strongly correlated with the injection signal. Using the 'real' injection signal shape, the event rate from numerically triggered microseismicity clouds is computed. The result is shown in figure 4.9b. For comparison, the measured event rate during this experiment is shown once more in figure 4.9c. Obviously, the numerically triggered events and the real observation show significant similarity. The numerically simulated triggering process qualitatively and quantitatively yields the same correlations with the injection function. The comparison shows that our numerical modeling approach is suitable for the simulation of real injection experiments. The event rate observed is comparable to the real measured one despite of the simple homogeneous model used.

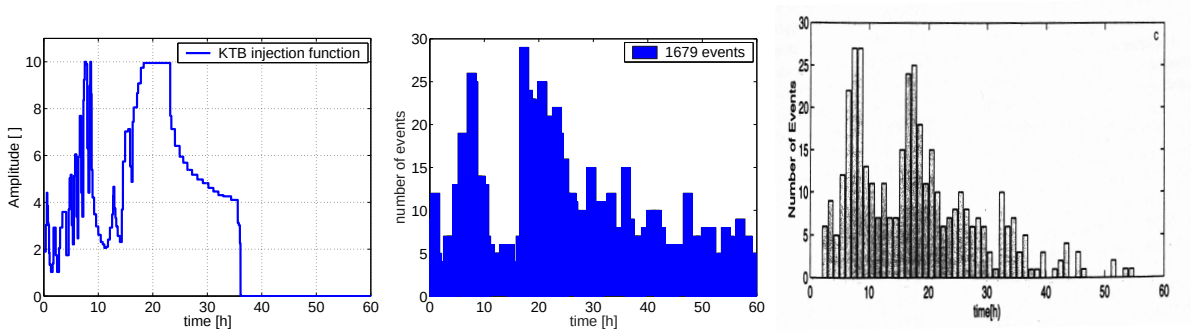

(a) (b) (c)

Figure 4.9: (a) Source function used for modeling in a hydraulically homogeneous and isotropic 3D medium. Interpolation of the signal was done according to the real injection signal measured during the 1994 experiment (see Zoback and Harjes [1997b]. (b) Event rate for a cloud consisting of 1679 events after numerical triggering. (c) Event rate observed during the 1994 injection experiment at the KTB.

4.6.2 Hydraulic model from reflectivity

As already pointed out, the subsurface at the German KTB drilling site is dominated by strong heterogenity. The variations in seismic reflection amplitudes are significant, correlating with fluctuations in seismic velocities. As proposed in chapter 4.4, the increased seismic reflection amplitudes can correlate with increased natural fracture densities also. A larger amount of pre-existing fractures effect also hydraulic properties of the rock. Therefore, increased seismic reflection intensities can also correlate with an increased hydraulic diffusivity or permeability.

In order to study the process of pressure perturbation within a complex medium like at the

KTB, the fluid injection in a heterogeneous model is simulated. For the hydraulic FEM model, an interpolated diffusivity field was used. This field was interpolated from the real seismic reflection measurements. A 2D model with hydraulic diffusivity varying between D_{min}=5 m^2/s and D_{max} =50 m^2/s is used. The normalized reflection amplitudes of the 3D migration profile (see Buske [1999] and compare figure 4.5b) for the *xy*-slice passing through the borehole location (y=10.4 km) are computed. A threshold-criterion is used to define the hydraulically homogeneous background and the variations in diffusivities. The strong reflections from the SE1 reflector as well as from the Erbendorf body are defined as a 10 times increased hydraulic diffusivity compared to the background value in this model as a first rough approximation. This increase is assumed to be reasonable for differences in hydraulic properties for consolidated and highly fractured rocks (Kaselow, pers. comm.).

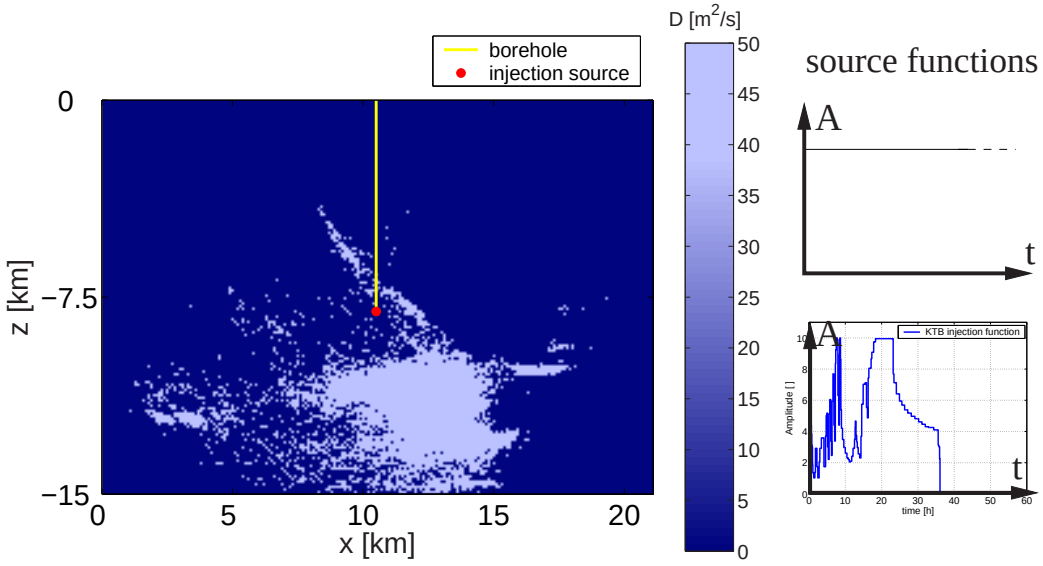

Figure 4.10: Hydraulic model used for numerical simulation. Colors correspond to hydraulic diffusivities, the yellow solid line represents the main KTB borehole. The red circle denotes the injection source point.

The injection source point is defined at the position, where the real injection took place in 1994 at approximately 9.0 km depth. As source function a step function of constant amplitude as well as the source function shown in figure 4.9a is used. The model set-up is shown in figure 4.10. The yellow solid line represents the main KTB borehole, the red circle the injection source point. Colors correspond to the hydraulic diffusivities used for modeling. On the right side of figure 4.10 the source functions used for simulation are shown.

In figure 4.11 the time-dependent pressure perturbation within the model shown in figure 4.10 and a step-function-like source signal are displayed. The perturbation modeled using the real source function of the 1994 injection experiments is shown in figure 4.12. Colors correspond to the pressure amplitudes and solid lines to isolines of constant pressures, respectively. The results clearly show the preferential propagation of high pressures within the high-diffusive (high-reflective) structures corresponding to the seismic SE1 reflector

and the EB zone. Even after the source function is turned off the increased pressure within these high-diffusive regimes is clearly observable.

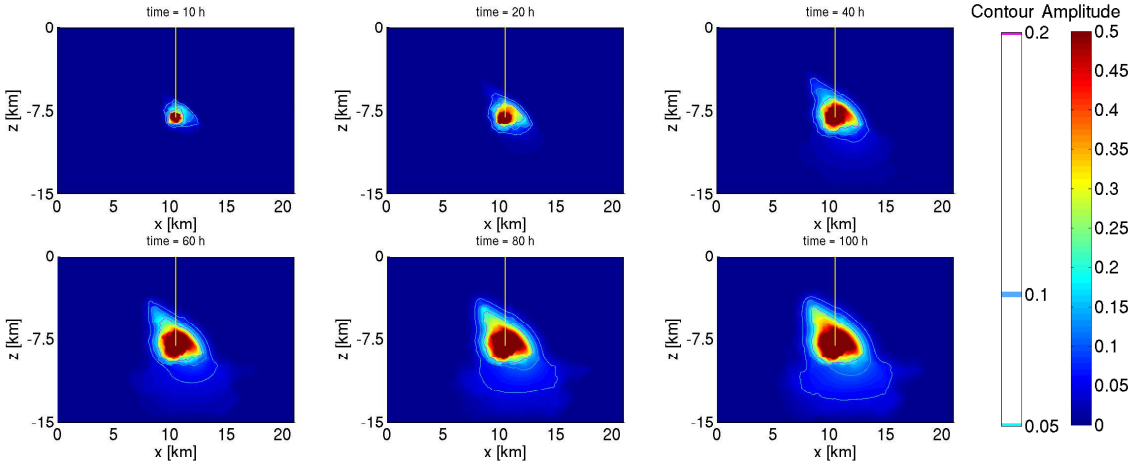

Figure 4.11: Time-dependent solution of pore pressure perturbation for the numerically simulated hydraulic KTB model using a step-function-like injection source. Colors correspond to pressure amplitudes, solid lines to isolines of constant pressures. The yellow solid line denotes the KTB main borehole. The red circle corresponds to the position of the injection point in the model.

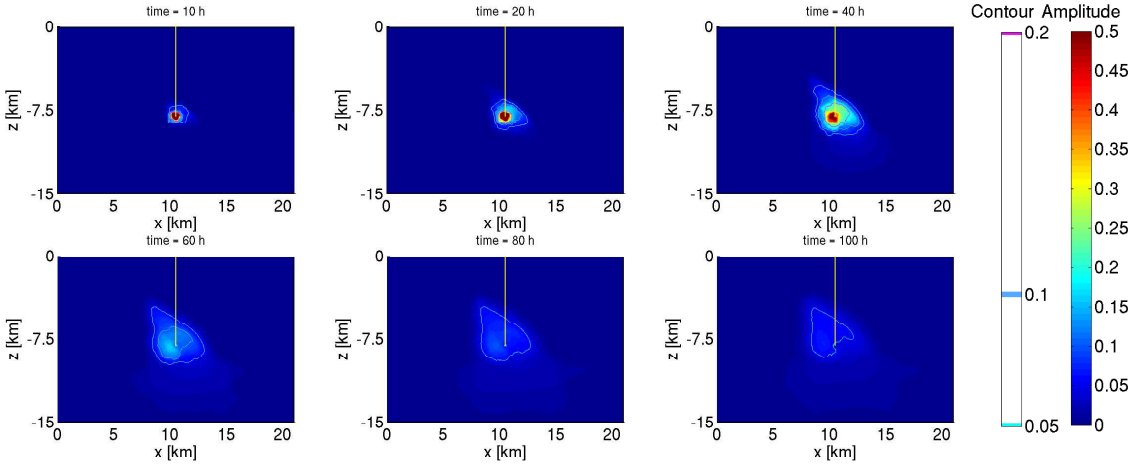

Figure 4.12: Time-dependent solution of pore pressure perturbation for the numerically simulated hydraulic KTB model using the real 1994 injection source function (figure 4.9a). Colors correspond to pressure amplitudes, solid lines to isolines of constant pressures (see caption in figure 4.11). The yellow solid line denotes the KTB main borehole. The red circle corresponds to the position of the injection point in the model.

For numerical triggering of events, criticality was firstly evenly distributed between $0< C <50$ and source amplitude was set to A=10, corresponding to a stable medium with respect to the state of critical stresses. After numerical triggering, the complete seismicity cloud consists of 134 events, occurring mainly within the high-diffusive SE1 structure as well as within the EB body. According to the observations at the KTB in 1994, events occurring at depths z <-10km are removed for the analysis (compare chapter 4.1). The residual cloud consists of 58 events comparable with the 94 events observed in 1994. The

simulated event cloud is shown in figure 4.13a, the hypocenter locations of the cloud observed in 1994 together with reflection seismic results are shown in figure 4.13b.

Two main similarities of numerical and real data are observable denoted with numbers 1 and 2 in figure 4.11: at first, the spherical clustering of seismicity occurring around the injection source (denoted with 1) and secondly, the preferential alignment of hypocenters along the structures of the SE1 reflector (denoted by 2). In the numerical model, a larger number of events was induced around the highly diffusive SE1 zone than observed during the experiment. Two explanations for the latter are possible: Either the numerical model was still too critical in terms of critical stresses or - during the experiment and localization in 1994 - the seismicity also occurred at these depth regimes but could not be located precisely enough to be included in the data set.

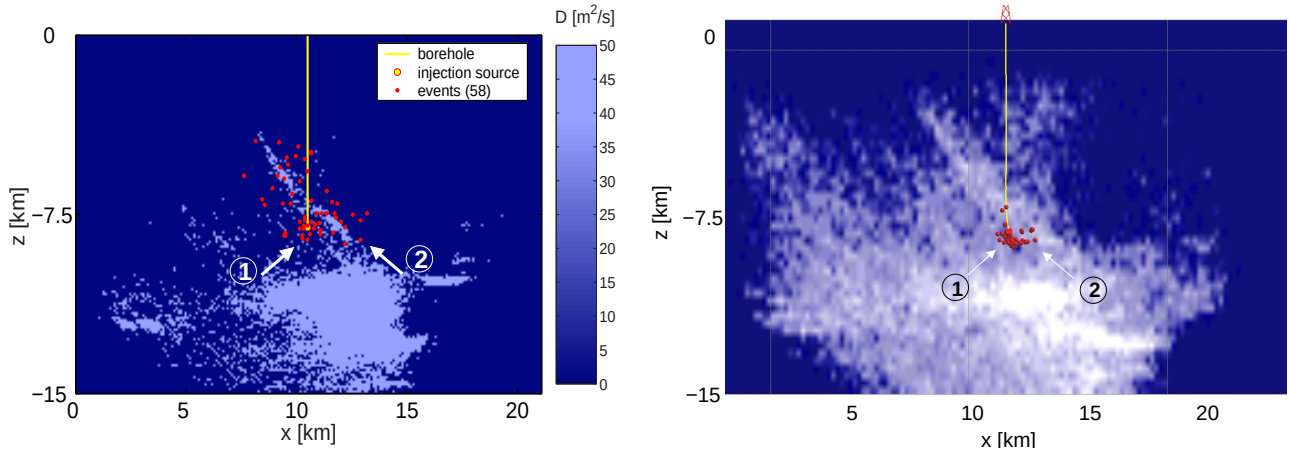

(a) (b)

Figure 4.13: (a) Hydraulic model used for simulation together with the event cloud induced after numerical triggering. Blue colors correspond to hydraulic diffusivities used for modeling. (b) Hypocenter locations of events observed in 1994 (Zoback and Harjes [1997a]; Jost et al. [1998]). Colors correspond to the seismic reflection amplitudes. In both figures, the spherical clustering of events around the injection source (1) as well as the preferential alignment of hypocenters along the dominant SE1 structure (2) is visible.

For the analysis of the event rate, criticality C was evenly distributed between zero and ten within the model. The source function shown in figure 4.9a was used. A total amount of 817 events was triggered shown in figure 4.14a. Obviously, events predominantly cluster along the high-diffusive regimes defined in the hydraulic model. Moreover, events mainly occur in the depth range down to $z \approx$-9km (71.2% of events occur at depths $0 > z >$-9km). However, about 28.8% of events are triggered below the depth of the KTB open hole section because of the hydraulic coupling between the SE1 structure and the EB in the model. For the 1994 experiment no event was observed at these depth intervals. For the injection experiment of 2000, a few isolated events at larger depths were observed. Baisch and Harjes [2003] explained these events with fluid migration along highly permeable fracture branches at comparably low fluid pressure elevations. Nevertheless, it is not clear to what

extend fluid migration at larger depths is possible by the ambient conditions at the KTB.

The estimation of effective scalar hydraulic diffusivity using equation (2.6) of the SBRC approach is shown in figure 4.14b. The spatio-temporal distribution of the events is shown together with four envelopes calculated with hydraulic diffusivities of D=3, 5, 10 and 50 m^2/s, respectively. The hydraulic diffusivities observed from numerical modeling give two main results: first, the envelope calculated with the hydraulic diffusivity D=50 m^2/s used in the model also corresponds to the upper envelope for the events as predicted by the SBRC approach. Secondly, more than 73 % of events are located below the envelope calculated with a hydraulic diffusivity of D=5 m^2/s, correlating with the values of diffusivity observed for the data of the 1994 experiment (compare with figure 4.4a). The percentage of events located below the envelopes shown in figure 4.14b are given in table 4.1 below. Numerical simulation therefore supports the values of hydraulic parameters estimated from real data despite of the simplicity of the model used.

	D=3 m^2/s	D=5 m^2/s	D=10 m^2/s	D=50 m^2/s
events below D [%]	61.1	73.3	87.1	99.8

Table 4.1: Percentages of events located below the envelopes shown in figure 4.14b.

The event rate for this data set is shown in figure 4.9b. The comparison with the event rate observed during the real injection experiment in 1994 (figure 4.9c) again shows remarkable similarities: Two peaks of events occur at the maxima of the injection source function. The increase and decrease of event numbers before t=8h and after t=25h are comparable as well.

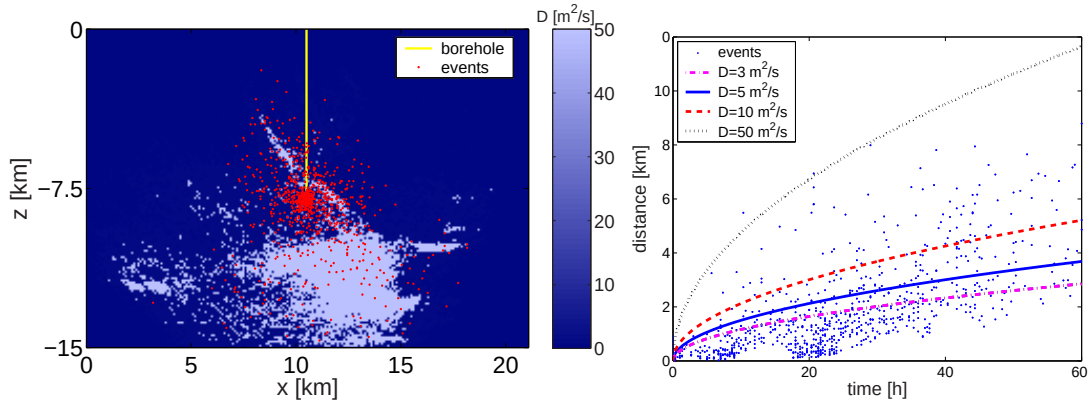

(a) (b)

Figure 4.14: (a) Cloud of events of the numerical modeling. A total of 817 events was triggered. (b) Estimation of effective scalar hydraulic diffusivity using the SBRC approach.

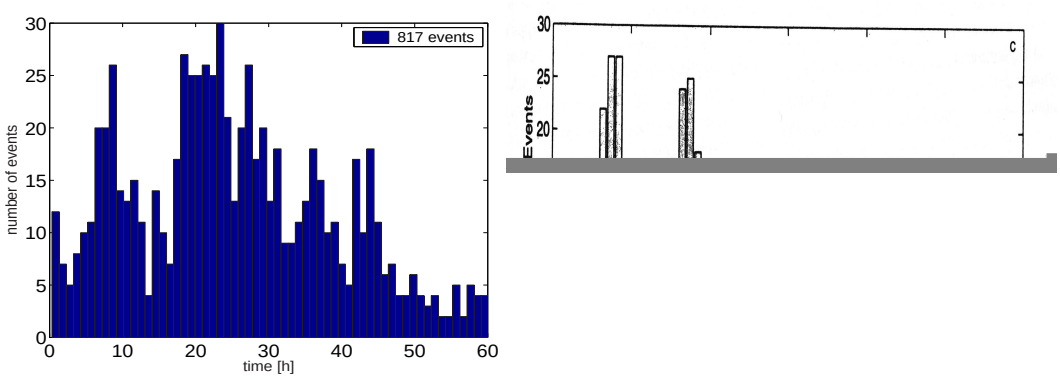

Figure 4.15: (a) Event rate for the data shown in figure 4.14. (b) Event rate for real data observed during the fluid injection experiments at the KTB in 1994.

Results of modeling

From numerical modeling it turns out that

- a variation of hydraulic diffusivities between high-reflective and low-reflective zones of a factor of 10 seems to be reasonable to explain observed microseismic events and their spatio-temporal evolution at the KTB.
- If the hypothesis is valid, that the high-reflective zones in the subsurface at the KTB are characterized by a one order of magnitude higher diffusivity than the surrounding rock, than the medium does not necessarily have to be in a critical state of stress in order to trigger seismicity comparable with real observations.
- It is possible to explain the rate of events as well as the spatial distribution of hypocenters.
- By simulating the injection source function of the 1994 experiment at the KTB and an interpolated 2D heterogeneous hydraulic model, similar clouds of events like in reality are observed.
- Events occur at larger depths than observed in 1994 during the experiment. This is due to the fact that in the model the high-reflective zones SE1 and EB are also hydraulically coupled.
- Observations in 2000 of few events occurring at larger depths support the hypothesis of hydraulic coupling between the different structures. This is also supported by the combined analysis of microseismicity and 3D reflectivity results and the modeling shown here.
- Estimations of effective scalar hydraulic diffusivity using numerical data support the observations from real data.

4.7 Conclusion

By analyzing data of two fluid-injection experiments at the KTB it was possible to estimate values of hydraulic diffusivities in situ for two different depth intervals at the same site. The influence of the orientations of pre-existing natural fracture systems on the triggering of microseismicity is obvious. Shallower seismic clouds show more compact shapes. The results are compared with images obtained by 3D prestack Kirchhoff depth migration. The decreased hydraulic diffusivity is correlated with a region of decreased reflectivity. Furthermore, the magnitude of hydraulic diffusivity at the shallower level is significantly smaller than that at the deeper level, where the hypocenters seem to be distributed along preferred orientations of natural fractures. The medium at this depth is characterized by a much higher diffusivity, correlating with larger reflectivity. This is expected to be observable in different environments as well. Numerical modeling results support the hypothesis that fluids at the KTB play an important role in the triggering of seismicity. With the modeling approach presented in this thesis, it is possible to simulate both event rates and hypocenter locations. These experiments can potentially help to improve further injection experiments planned at the KTB site.